

Supplementary Material for the article: Photonic bands, superchirality, and inverse design of a chiral minimal metasurface

Simone Zanotto and Alessandro Pitanti
*Istituto Nanoscienze - CNR and Laboratorio NEST,
Scuola Normale Superiore, Piazza San Silvestro 12, 56127 Pisa, Italy**

Giacomo Mazzamuto and Francesco Riboli
*European Laboratory for Non Linear Spectroscopy,
via N. Carrara 1, Sesto Fiorentino, Firenze 50019, Italy and
CNR-INO Sesto Fiorentino, via Nello Carrara 1, Firenze 50019, Italy*

Giorgio Biasiol
Istituto Officina dei Materiali CNR, Laboratorio TASC, Basovizza (TS) - Italy

Giuseppe C. La Rocca
Scuola Normale Superiore and CNISM, Piazza dei Cavalieri 7, 56126 Pisa, Italy

Alessandro Tredicucci
*Istituto Nanoscienze - CNR and Laboratorio NEST,
Scuola Normale Superiore, Piazza San Silvestro 12, 56127 Pisa, Italy* and
Dipartimento di Fisica “E. Fermi”, Università di Pisa, Largo Pontecorvo 3, 56127 Pisa, Italy
(Dated: October 10, 2019)*

This Supplementary Material provides details on the metasurface fabrication process, on the numerical calculations, on the algebraic properties of the T -matrix singular value decomposition, and datasets containing the inverse problem solutions.

METASURFACE FABRICATION

The metasurface samples have been fabricated starting from a GaAs wafer, where an epitaxial bilayer consisting of $\text{Al}_{0.5}\text{Ga}_{0.5}\text{As}$ (1500 nm) and GaAs (220 nm) has been deposited. Several L-shaped hole arrays have been defined by means of e-beam lithography on a $8\text{ mm} \times 8\text{ mm}$ chip (Zeiss Ultraplus SEM + Raith Multibeam lithography system; 30 keV, AR-P 6200 resist). The pattern has then been transferred on the semiconductor layer by means of ICP-RIE with $\text{Cl}_2/\text{BCl}_3/\text{Ar}$ gas mixture (Sentech). To obtain the patterned membrane, the chip has been etched from the back side with a sequence of wet etching steps. First, a fast etching ($\text{H}_2\text{SO}_4:\text{H}_2\text{O}_2:\text{H}_2\text{O}$, 1:8:1) with $\approx 10\text{ }\mu\text{m}$ per minute etch rate is employed to thin the substrate down to $\approx 50\text{ }\mu\text{m}$. A resist mask (S1818) is employed in order to protect $\approx 1\text{ mm}$ of chip on the edges, thus allowing for chip handling. Second, a slow etching (3:1 solution of citric acid in 30% hydrogen peroxide; citric acid is prepared in 1:1 weight ratio with water) having $\approx 1\text{ }\mu\text{m}$ per minute etch rate is employed to remove all the remaining GaAs substrate. This solution is selective and stops when the $\text{Al}_{0.5}\text{Ga}_{0.5}\text{As}$ layer is reached. In this phase a second resist mask is employed, in order to realize membranes of $\approx 800\text{ }\mu\text{m} \times 800\text{ }\mu\text{m}$ size. Finally, an HF bath (50% concentration) is employed to remove the $\text{Al}_{0.5}\text{Ga}_{0.5}\text{As}$ layer and obtain the frame-supported patterned membrane (Fig. S1). During the first two wet etching steps the chip is mounted on a

glass slide by means of S1818 resist.

NUMERICAL CALCULATIONS

The transmission matrix (Jones matrix) of the metasurface has been calculated by means of Periodically Patterned MultiLayer (PPML), a MATLAB software that implements the rigorous coupled wave analysis scattering matrix method (RCWA) following the formalism of [1–4]. In particular, we employed the **ZSM-2d-Lshape** function that calculates the zero-diffraction-order scattering matrix (i.e., the polarization-resolved reflection and transmission matrices) of the metasurface[5]. The theoretical spectra in Figs. 1 and 2 have been smoothed by convolution with a 2 nm wide Gaussian in order to better compare them with the experimental ones.

The field plots reported in Fig. 2 of the main text have instead been made with the finite-element software COMSOL.

EMPTY LATTICE BAND DISPERSION

To understand the nature of the dispersive features observed in the angularly-resolved circular dichroism spectra reported in the main text, we performed an empty-lattice band dispersion calculation. First we identified the guided modes supported by an unpatterned dielectric

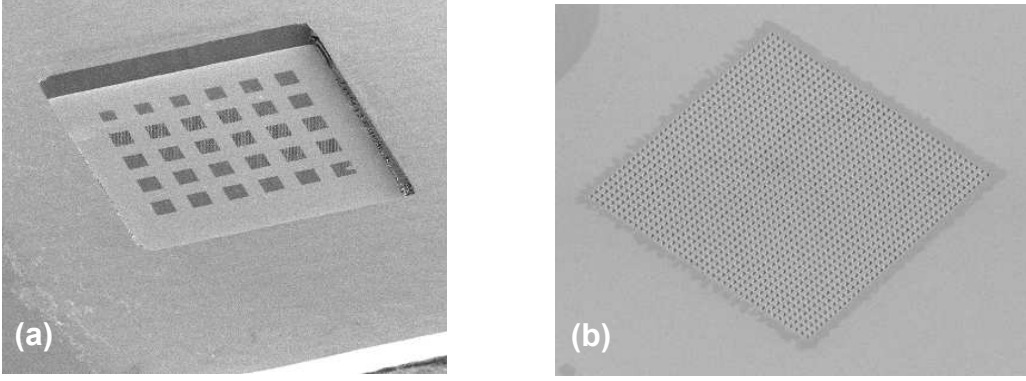


FIG. 1. Scanning electron microscope images of the fabricated metasurface sample. (a) An $800\ \mu\text{m} \times 800\ \mu\text{m}$ sized membrane containing a group of L-shaped hole arrays. The chip is here observed from the bottom side. (b) A single L-shaped hole array, of size $50\ \mu\text{m} \times 50\ \mu\text{m}$.

slab, whose thickness and refractive index is the same as that of the gallium arsenide slab employed to fabricate the metasurface. The modal effective refractive indices (n_{eff}) are reported in Fig. S2a: in the wavelength range of interest the slab supports the fundamental TE and TM modes (TE_0 and TM_0) and, below the cutoff wavelength of $\approx 1.4\ \mu\text{m}$, also the first-order modes. As the TM_1 mode has a very low value of n_{eff} , the plot reports only the TE_1 mode. Second, we folded the guided modes in the first Brillouin zone, according to the zero-order perturbation theory summarized by the equation

$$|\mathbf{k}_B + \mathbf{g}| = \beta$$

where \mathbf{k}_B is the Bloch wavevector, \mathbf{g} is a reciprocal lattice vector, and β is the guided mode propagation constant (i.e., $\beta = 2\pi n_{\text{eff}}/\lambda$) [6]. Consistently with the experiments, the Bloch wavevector is varied within the first Brillouin zone along the high-symmetry direction indicated in Fig. S2b. The resulting mode dispersions are reported in Fig. S2c; notice that they appear symmetric since no symmetry-breaking mechanisms are encoded in this simple model. Despite the simplicity of the model, a comparison between theory and experiment (i.e., between Figs. S2c-d) shows that the overall trend of the features observed in the experiment are appropriately grasped by the model. This confirms that the dispersive bands observed in the transmission spectra, and hence in the circular dichroism spectra, originate from a guided-mode resonance mechanism.

DEMONSTRATION OF THE ALGEBRAIC STRUCTURE OF T -MATRIX SINGULAR VALUE DECOMPOSITION

In Sect. 5 of the main text we reported that the T -matrix of a metasurface belonging to the $M_{x,y}$ symmetry class can be expressed by means of singular value

decomposition (SVD) in a specific form. We briefly outline here the demonstration of that result. First, we recall that any complex matrix M can be decomposed in the form $M = U_1 \Sigma U_2^\dagger$, where $U_{1,2}$ are unitary matrices whose columns are the (right and left) singular vectors of M , and Σ is a diagonal matrix whose entries are real non-negative numbers (the singular values) [7]. The SVD plays an important role in the theory of linear multiport lossy optical components, since the singular values are the minimum and maximum absorption levels that the component can implement [8].

First observation is that the SVD of T_L , which is a symmetric matrix by hypothesis ($T_L = T_L^\dagger$), can be cast to a special form. Indeed, from the above definition it turns out that one can write $T_L = \bar{U} \Sigma U^\dagger$, where the bar indicate the element-wise matrix complex conjugate. Matrix T_C is obtained from T_L by the linear-to-circular basis conversion matrix [9], i.e., $T_C = \Lambda^\dagger T_L \Lambda$, where $\Lambda = \frac{1}{\sqrt{2}} \begin{pmatrix} 1 & 1 \\ i & -i \end{pmatrix}$. Looking for a SVD of T_C , i.e., for an expression $T_C = V \Sigma W^\dagger$, it turns out immediately that V and W must satisfy $\bar{V} W = \begin{pmatrix} 0 & 1 \\ 1 & 0 \end{pmatrix}$. By inspection we obtained the decomposition of V and W in more elementary matrices that is reported in the main text.

COMPLETE DATASET OF METASURFACE SHAPE PARAMETERS NEEDED TO TARGET ARBITRARY FUNCTIONS

In Sect. 6 of the main text we claimed that, by appropriately shaping the L-shaped hole, an arbitrary T -matrix can be obtained. The problem has been approached numerically by defining an error function that quantifies the distance of the T -matrix of a metasurface with certain geometrical parameters (i.e., $T(a, f_1 \dots f_4)$) from the target T -matrix (i.e., T_{targ}). According to the matrix parametrization given in Sect. 5, the error func-

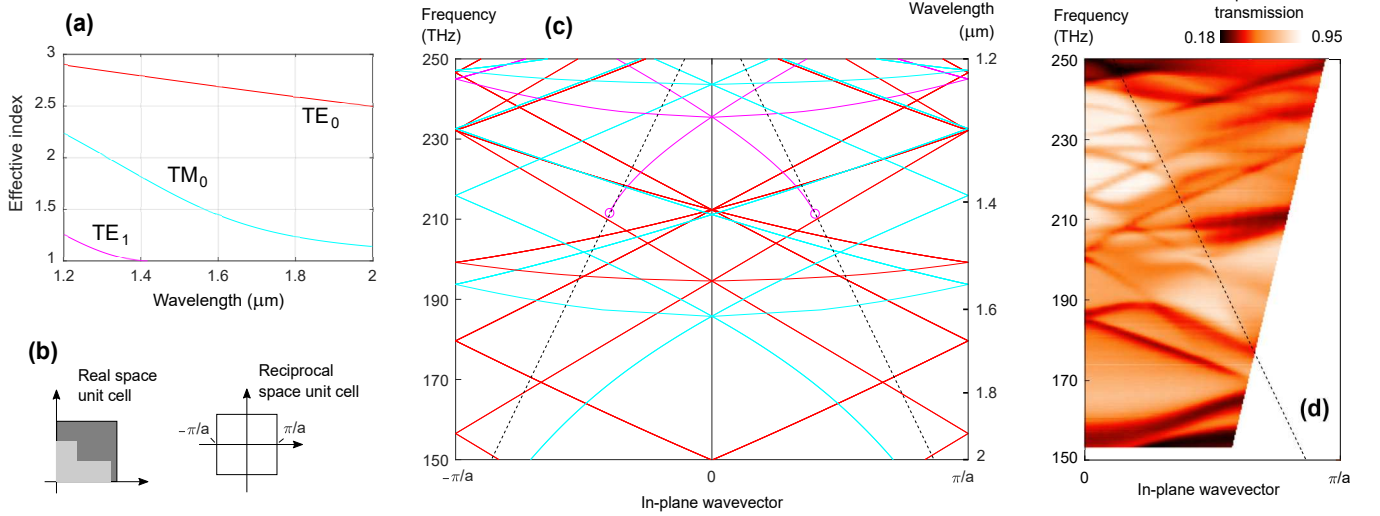


FIG. 2. Empty lattice band dispersion from the guided modes of a dielectric slab. Panel (a), effective index dispersion for the unpatterned slab guided modes. Panel (b), real space unit cell (i.e., a square unit cell enclosing the L-shaped hole) and reciprocal space unit cell (i.e., first Brillouin zone). Panel (c), band dispersion originating from the mode folding. The circles at $\approx 1.4\mu\text{m}$ indicate the TE_1 cutoff; the diagonal dashed line represent the diffractin threshold (i.e., the folded air light cone). Panel (d), experimental unpolarized angle-resolved transmission.

tion is defined as

$$\begin{aligned} \text{error} = & (\sigma_1 - \sigma_{1,\text{targ}})^2 + (\sigma_2 - \sigma_{2,\text{targ}})^2 + \\ & + \left(\left(S_3^{(1)} - S_{3,\text{targ}}^{(1)} \right) / 2 \right)^2 + \\ & + \sin^2 \left(\frac{2\Delta - 2\Delta_{\text{targ}}}{2} \right) + \sin^2 \left(\frac{\phi - \phi_{\text{targ}}}{2} \right) \end{aligned}$$

and it is used in an optimization process that employs the `fmincon` function of the Optimization Toolbox of MATLAB. Notice that we employed 2Δ rather than Δ , since it is the former which has physical significance (see the main text). The constraints on the geometric parameters are the following: $a \in [0.8, 1.5] \mu\text{m}$, $f_{1..4} \in [0.2, 0.9]$, $f_3 < f_1$, $f_4 < f_2$. For each target, several optimization processes with random starting points were needed in order to get a solution within an acceptable error level ($\text{error} < 0.02$).

While approaching the process of targeting arbitrary metasurface functions, one might extract random combinations of target $\sigma_{1,\text{targ}}$, $\sigma_{2,\text{targ}}$, $S_{3,\text{targ}}^{(1)}$, Δ_{targ} and ϕ_{targ} and solve the inverse problem. However, further analysis on the meaning of these parameters suggests that certain subsets deserve more relevance than others. For instance, the combinations where $\sigma_{1,\text{targ}} = 1$ and $\sigma_{2,\text{targ}} = 1$ can be excluded from the present analysis. Indeed, this request means that the T -matrix must be unitary, and that its eigenvectors must be orthogonal. However, following [10], the T -matrix of an $M_{x,y}$ object has corotating eigenvectors; merging this requirement to that of eigenvector orthogonality means that the eigenvectors must be linearly polarized. This observation implies that there is no need to employ an L-shaped structure; a simpler rotated

rectangular or elliptical hole in a dielectric slab (or dielectric post on a substrate) will be sufficient to implement the required operation (see, for instance, the Supplementary Information of [11]). For this reason we will not consider the case $\sigma_{1,\text{targ}} = \sigma_{2,\text{targ}} = 1$. Another point to be observed is that it is sufficient to consider positive values of $S_{3,\text{targ}}^{(1)}$. Indeed, given a structure with geometrical parameters $[a, f_1, f_2, f_3, f_4]$ whose SVD parameters are $[\sigma_1, \sigma_2, \Delta, \phi, S_3^{(1)}]$, the structure obtained by exchanging $f_1 \leftrightarrow f_3$, $f_2 \leftrightarrow f_4$ (i.e., the enantiomer), will have the sign of $S_3^{(1)}$ inverted.

A first subset that deserve particular interest is that where one of the singular values is zero: $\sigma_{2,\text{targ}} = 0$; this set contains polarizers. It should be noticed that in this subset the parameters Δ is irrelevant, since in the final expression of the transmission matrix ($T_C = V\Sigma W^\dagger$) it only appears in the term $e^{-i(2\Delta - \phi)} = e^{-i(\phi + \pi)}$. We chose 24 combinations of target parameters within this set, that are reported in Table 3. In correspondence to each target, the table reports the values of the geometrical parameters that solve the inverse problem. In Table 3 we labeled with the letters a-c the first three cases considered in Fig. 6 of the main text.

The second subset that has been considered is that where both singular values are non-zero, but not simultaneously equal to unity. Within this subset we chose 96 target combinations, by allowing the target parameters to assume the values $\sigma_1 = 0.6, 1$; $\sigma_2 = 0.4$; $2\Delta = 0, \pi/4, \pi/2, 3\pi/4$; $\phi = 0, \pi/2, \pi, 3\pi/2$; $S_3^{(1)} = 0, 0.5, 1$. We have limited the range of 2Δ within the interval $[0, \pi]$ since it can be shown that a certain pair of 2Δ

σ_1	σ_2	2Δ	φ	$S_3^{(1)}$	a	f_1	f_2	f_3	f_4
0.6	0	0	0	0	0.9938	0.8330	0.7978	0.5392	0.6662
0.6	0	0	0	0.5	1.3443	0.7674	0.7907	0.5675	0.3304
0.6	0	0	0	1	1.1687	0.7088	0.4829	0.4714	0.3406
0.6	0	0	$\pi/2$	0	1.2440	0.7615	0.7351	0.4262	0.2813
0.6	0	0	$\pi/2$	0.5	1.2445	0.7514	0.7251	0.4223	0.3084
0.6	0	0	$\pi/2$	1	1.1854	0.7368	0.5343	0.3648	0.3610
0.6	0	0	π	0	1.2336	0.6270	0.7602	0.5406	0.2576
0.6	0	0	π	0.5	1.1836	0.4972	0.7687	0.3543	0.2777
0.6	0	0	π	1	1.1306	0.4772	0.6257	0.2662	0.3169
0.6	0	0	$3\pi/2$	0	1.3239	0.7363	0.7359	0.6627	0.3907
0.6	0	0	$3\pi/2$	0.5	1.1779	0.6978	0.5316	0.4554	0.4257
0.6	0	0	$3\pi/2$	1	1.2201	0.7853	0.5633	0.4672	0.4572
1	0	0	0	0	1.3973	0.8076	0.7894	0.5026	0.4428
1	0	0	0	0.5	1.2332	0.5316	0.7479	0.4218	0.5039 (c)
1	0	0	0	1	1.3110	0.6198	0.8015	0.2802	0.5743 (a)
1	0	0	$\pi/2$	0	1.3050	0.8068	0.8127	0.5881	0.4393
1	0	0	$\pi/2$	0.5	1.2848	0.6696	0.8484	0.3006	0.3520
1	0	0	$\pi/2$	1	1.2145	0.5670	0.7241	0.3332	0.4082
1	0	0	π	0	1.2181	0.7213	0.7034	0.3501	0.3843
1	0	0	π	0.5	1.2560	0.7885	0.7583	0.3781	0.2567
1	0	0	π	1	1.2365	0.7688	0.7021	0.3309	0.2806 (b)
1	0	0	$3\pi/2$	0	1.2949	0.7338	0.7386	0.6217	0.2357
1	0	0	$3\pi/2$	0.5	1.1899	0.5556	0.8793	0.2314	0.3901
1	0	0	$3\pi/2$	1	1.3379	0.7858	0.8095	0.5287	0.3638

FIG. 3. Target parameters and corresponding geometrical parameters that solve the inverse problem. In the present subset, where $\sigma_2 = 0$, the value of 2Δ is irrelevant (see text). The lines marked with a letter are the cases reported in Fig. 6 of the main text.

and ϕ leads to the same T -matrix obtained by employing $2\Delta + \pi$ and $\phi + \pi$. The inverse problem has been solved successfully for all the 96 combinations. However, an illustrative subset is reported in Table 4, where a random sampling of the complete dataset has been listed. Here, the letter “d” labels the fourth case considered in Fig. 6 of the main text. The complete dataset is available on the author’s webpage[12]. In the data of Tables 3 and 4 there is not immediate evidence of a correlation between the target parameters and the geometrical parameters; however, more refined data analysis techniques and finer-grained parameter sweeping may reveal more details of the physics behind the inverse problem. However, the study of these aspects goes beyond the aims of the present work and may be the topic of future research.

* simone.zanotto@nano.cnr.it

- [1] D. M. Whittaker and I. S. Culshaw, Scattering-matrix treatment of patterned multilayer photonic structures, *Phys. Rev. B* **60**, 2610 (1999).
- [2] M. Liscidini, D. Gerace, L. C. Andreani, and J. E. Sipe, Scattering-matrix analysis of periodically patterned multilayers with asymmetric unit cells and birefringent media, *Phys. Rev. B* **77**, 035324 (2008).
- [3] L. Li, Use of fourier series in the analysis of discontinuous periodic structures, *J. Opt. Soc. Am. A* **13**, 1870 (1996).
- [4] P. Lalanne and G. M. Morris, Highly improved convergence of the coupled-wave method for tm polarization, *J. Opt. Soc. Am. A* **13**, 779 (1996).
- [5] The code is available at <https://it.mathworks.com/matlabcentral/fileexchange/55401-ppml-periodically-patterned-multi-layer>.
- [6] S. Collin, Nanostructure arrays in free-space: optical properties and applications, *Reports on Progress in Physics* **77**, 126402 (2014).
- [7] R. A. Horn and C. R. Johnson, *Topics in Matrix Analysis* (Cambridge University Press, 1991).
- [8] L. Ge and L. Feng, Contrasting eigenvalue and singular-value spectra for lasing and antilasing in a \mathcal{PT} -symmetric periodic structure, *Phys. Rev. A* **95**, 013813 (2017).
- [9] In the notation we employ, circular polarization basis is sorted according to (RCP,LCP). RCP is defined as following: at fixed position in space, the electric vector rotates in the sense dictated by the fingers of a right hand whose thumb is pointing along the propagation direction. Moreover, we use the convention $e^{-i\omega t}$.
- [10] C. Menzel, C. Rockstuhl, and F. Lederer, Advanced jones calculus for the classification of periodic metamaterials, *Phys. Rev. A* **82**, 053811 (2010).
- [11] A. Arbabi, Y. Horie, M. Bagheri, and A. Faraon, Dielectric metasurfaces for complete control of phase and polarization with subwavelength spatial resolution and high transmission, *Nature nanotechnology* **10**, 937 (2015).
- [12] The dataset is available at <http://meta.nano.cnr.it>.

σ_1	σ_2	2Δ	φ	$S_3^{(1)}$	a	f_1	f_2	f_3	f_4
0.6	0.4	0	0	0	1.2826	0.8716	0.5444	0.8060	0.5215
0.6	0.4	0	$\pi/2$	0.5	1.1656	0.5322	0.6821	0.2828	0.3505
0.6	0.4	0	π	0	1.2528	0.7001	0.7352	0.5685	0.2487
0.6	0.4	0	π	0.5	1.3148	0.8575	0.8210	0.4721	0.3737
0.6	0.4	0	$3\pi/2$	1	1.1737	0.7502	0.5052	0.3574	0.2555
0.6	0.4	$\pi/4$	0	0.5	1.1741	0.7125	0.5190	0.4399	0.3339
0.6	0.4	$\pi/4$	0	1	1.3281	0.8364	0.7149	0.3975	0.6206
0.6	0.4	$\pi/4$	π	1	1.1451	0.3764	0.8598	0.2487	0.3295
0.6	0.4	$\pi/2$	0	0	1.3302	0.7199	0.7260	0.6169	0.5742
0.6	0.4	$\pi/2$	$\pi/2$	0.5	1.2684	0.8018	0.7191	0.2910	0.2847
0.6	0.4	$\pi/2$	π	0.5	1.2120	0.7595	0.6852	0.2727	0.5162
0.6	0.4	$3\pi/4$	$\pi/2$	1	1.2718	0.6901	0.7928	0.2914	0.3340
0.6	0.4	$3\pi/4$	π	0	1.1944	0.6169	0.7083	0.4198	0.4298
1	0.4	0	0	0.5	1.2016	0.7370	0.5177	0.4203	0.3813
1	0.4	0	0	1	1.3285	0.7816	0.7974	0.4874	0.3882
1	0.4	0	$\pi/2$	1	1.2470	0.7414	0.6727	0.3333	0.4634
1	0.4	0	π	1	1.2329	0.7730	0.6970	0.3173	0.2766
1	0.4	$\pi/4$	0	0.5	1.3117	0.8044	0.7260	0.4288	0.5364
1	0.4	$\pi/4$	$\pi/2$	1	1.2857	0.7245	0.7333	0.4874	0.3543
1	0.4	$\pi/2$	0	0.5	1.2840	0.7640	0.6205	0.5789	0.5215
1	0.4	$\pi/2$	$\pi/2$	0	1.4220	0.7826	0.8110	0.6344	0.6780
1	0.4	$\pi/2$	π	0	1.2317	0.7563	0.6795	0.5515	0.3512
1	0.4	$3\pi/4$	0	1	1.3204	0.8249	0.6625	0.6302	0.6176
1	0.4	$3\pi/4$	$\pi/2$	0.5	1.3136	0.7740	0.6230	0.4279	0.4207
1	0.4	$3\pi/4$	$3\pi/2$	0.5	1.1637	0.6183	0.5328	0.2784	0.4625

FIG. 4. Target parameters and corresponding geometrical parameters that solve the inverse problem. This table is an exemplary selection of a wider table, available upon request, that contains 96 combinations of target parameters and the corresponding geometrical parameters. The line marked with a letter is case “d” of the Fig. 6 of the main text.